Solar Energy Materials and Solar Cells 192 (2019) 57–64

Contents lists available at ScienceDirect

Solar Energy Materials and Solar Cells

journal homepage: www.elsevier.com/locate/solmat

A novel core-shell structural montmorillonite nanosheets/stearic acid composite PCM for great promotion of thermal energy storage properties

Hao Yi[a,b], Weiquan Zhan[b], Yunliang Zhao[a,b,*], Shuguo Qu[c], Wei Wang[a], Peng Chen[a], Shaoxian Song[a,b,*]

[a] Hubei Key Laboratory of Mineral Resources Processing and Environment, Wuhan University of Technology, 122 Luoshi Road, Wuhan, Hubei 430070, China
[b] School of Resources and Environmental Engineering, Wuhan University of Technology, 122 Luoshi Road, Wuhan, Hubei 430070, China
[c] College of Chemical Engineering, Qingdao University of Science & Technology, Qingdao, Shandong 266042, China

ARTICLE INFO

Keywords:
Phase change material
Montmorillonite nanosheet
Thermal energy storage
Microcapsule
Stearic acid

ABSTRACT

In this work, a novel nanocomposite phase change material (PCM) has been designed to greatly enhance the thermal energy storage capacity and thermal conductivity. It is the first time that two-dimensional montmorillonite nanosheets (2D-MMT) have been used in encapsulating stearic acid (SA) latex particles thus to prepare composite phase change materials (PCM), which is featured by the very thin shell and ultra-high content of active core materials. It was prepared through the self-assembly of positively charged MMT nanosheets on the negatively SA latex surfaces under a strong electrostatic attraction, leading to the formation of a core-shell structural composite PCM. The microstructure, thermal performances and cycling stability of this 2D-MMT/SA composites have been researched via Fourier transform infrared spectroscopy (FTIR), scanning electron microscope (SEM), differential scanning calorimetry (DSC), zeta potential measurement and thermal constant analyzer. The experimental results have shown that 2D-MMT/SA composite contained an ultra-high mass fraction (> 80%) of SA due to the very thin MMT nanosheets shell, thus to have a tremendous latent heat storage capacity (184.88 J/g). In addition, the thermal conductivity of this PCM composite can reach to 159.46% of SA at most on account of the relatively high thermal conductivity of MMT nanosheets. Moreover, the protective 2D-MMT shell provided an excellent shape stability to the composite thus to restrict the leakage of PCM effectively. The composite also exhibited a stable cycling performance in the heating/cooling test. It is demonstrated that this 2D-MMT/SA composite would be of great promise for solar energy storage in sustainable energy field because of the very low cost, ultra-high latent heat storage capacity, promoted thermal conductivity, excellent structural stability and outstanding cycling performance.

1. Introduction

The demand for renewable and clean energy is becoming more and more desperately urgent due to the energy exhaustion and environment pollution in the last few decades [1,2]. Solar energy is believed to be the most prospective energy for its environment friendly and renewable nature. However, solar energy can only be utilized in the daytime when there is sun, thus the technologies on solar energy storage are desperately needed before humans can take full advantage of solar energy. Phase change materials (PCM) have the ability to absorb solar radiation and transform into thermal energy, which can be stored during phase transition process [3,4], so it shows great potential for practical applications in storing solar radiant heat which are inexhaustible and eco-friendly [5–7]. Actually, due to its high thermal energy storage capacity as well as small temperature changes in the phase transition, PCM has already been widely employed in solar energy storage, and the stored thermal energy has been supplied for the energy consumption for air-conditioning, building energy cycle, temperature regulating textiles and electronic thermal control [8–12]. Therefore, develop the sustainable solar energy storage technologies, such as PCM, may be an effective measure to alleviate the energy crisis and the environmental problem [13,14].

Generally, composite PCM have to be prepared by using some supporting materials in order to prevent the leakage of PCM and keep the cyclic durability of composite PCM. However, some problems such as low thermal storage capacity, low thermal conductivity or high cost

* Corresponding authors at: Hubei Key Laboratory of Mineral Resources Processing and Environment, Wuhan University of Technology, 122 Luoshi Road, Wuhan, Hubei 430070, China.
E-mail addresses: zyl286@whut.edu.cn (Y. Zhao), ssx851215@whut.edu.cn (S. Song).

https://doi.org/10.1016/j.solmat.2018.12.015
Received 16 September 2018; Received in revised form 7 December 2018; Accepted 7 December 2018
Available online 17 December 2018
0927-0248/

still restricted the development and practical application of PCMs. For example, polymer based composite PCMs have poor thermal properties such as low thermal stability, poor thermal conductivity and weak mechanical strength [15–17]. Besides, the percent content of PCM in polymer/PCM composite is commonly very low (< 80%) considering that very thick shells of polymers are essential to restrict leakage effectively, which leads to very low thermal energy storage capacity [18,19]. In recent years, some graphene based composite PCMs have been reported and showed good thermal energy storage properties [20–23]. However, the difficult preparation method of graphene makes it hard to produce at large scale [24,25]. The high cost of graphene seriously restricted the development and application of graphene based composite PCM. By comparison, some mineral based PCM enables a relative stable structure because PCM can be stabilized by the capillary force [26]. However, for the limited pore or interlayer space, minerals based composite PCM has very low latent heat storage capacity on account of the low mass fractions of PCMs (< 80%). For example, Sarier et al. have prepared a MMT based composite PCM through intercalation method, the mass percentage of PCM is about 60% while the latent heat storage capacity is only 125 J/g [27]. This was the largest heat storage in the reported MMT based composite PCM, which were far less than graphene based PCM. Above all, these existing composite PCMs showed either poor thermal performance or high cost, which greatly restricted the practical application of PCM in solar energy storage field.

Therefore, it is urgently to design a composite PCM not only with large latent heat and high thermal conductivity, but also with very low cost and easy preparation methods before developing the PCM to real applications. Herein, we want to present a facile method to prepare core-shell structural composite PCM by using very low-cost natural minerals but with excellent energy storage properties such as very high thermal energy storage capacity and relatively high heat transfer rate. Montmorillonite, a very common layered clay mineral, which structure is that one layer of alumina octahedral sheet is sandwiched between two layers of silica tetrahedron. Isomorphous substitutions in the crystal structure results in net negative charge in layers, which is balanced by exchangeable cations in interlayers such as Na^+, K^+, Ca^{2+} and Mg^{2+} [28]. Due to very strong hydration ability of these exchangeable cations, water molecules penetrate into the layers and force the layers apart, which increase the MMT layer spacing. Considering this swelling property of MMT, it is easy to exfoliate into two-dimensional montmorillonite nanosheets (2D-MMT) just through physical method [29–33]. By using these 2D-MMT nanosheets to encapsulate PCM, composite PCMs with ultra-high mass percentage of PCMs (> 80%), resulted by ultra-thin shell materials, may be achieved. Besides, the microencapsulation PCM has small size, large specific surface which are beneficial to improve high heat transfer rate [34]. In addition, the absorbability of clay minerals are superb thus PCMs can be easily loaded on the surface of clay minerals through Van der Waals' interactions, electrostatic forces, hydrophobic attractions or hydrogen bonds [35]. Furthermore, the high mechanical stability and perfect flame retardation of clay minerals enable 2D-MMT/SA microcapsules to be structural and thermal stable [36]. Compared with polymer or graphene, montmorillonite (MMT) is excellent supporting material to load the PCM due to the very low cost, relatively high thermal conductivity, good organic compatibility, excellent absorbability and perfect flame retardation [36,37]. Although some MMT based composite PCM has been reported. However, almost all the reported papers are to intercalate the PCMs to the interlayer space of MMT, the low loading of PCM and the low thermal storage capacity seriously hindered the development and application of MMT based composite PCM.

Therefore, we aimed to present an easy way to prepare core-shell composite PCM with excellent thermal energy storage properties while only use very low cost MMT. This 2D-MMT/SA composite PCM are designed to have ultra-thin shell thus to dramatically increase the weight fraction of PCM materials and greatly promote the solar thermal energy storage capacity. At the same time, the relatively high thermal conductivity of MMT and large heat transfer area are expected to improve the thermal conductivity of composite PCMs. Having solved traditional problems such as low thermal storage capacity, low thermal conductivity or high cost in the application of PCM, the prepared 2D-MMT/SA composites in this work with perfect energy storage property, outstanding structural stability and excellent cycling performance would be of great promise for solar energy storage and industrial waste heat recovering in sustainable energy field.

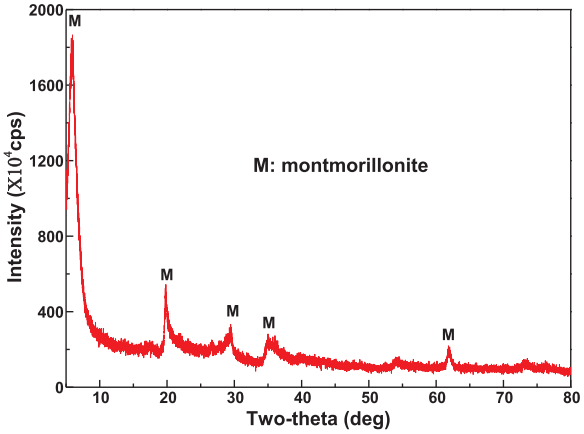

Fig. 1. XRD spectrum of montmorillonite.

2. Experiments

2.1. Materials

Montmorillonite were acquired from Chifeng Ningcheng Montmorillonite Company Limited (Inner Mongolia, China). Fig. 1 shows the X-ray diffraction spectrum (XRD) of montmorillonite, which demonstrated the high purity of MMT used in this work.

Stearic acid (SA), hexadecyl trimethyl ammonium bromide (CTAB) and sodium dodecyl sulfate (SDS) used in this work were of analytically pure. All these reagents were bought from the Sinopharm Chemical Reagent Company Limited in China. Water solution used in the whole experimental were ultra-pure water with the electrical resistivity of 18.2 MΩ cm, which were produced by Milli-Q ultra-pure water meter.

2.2. Methods

First, the MMT has been exfoliated to 2D-MMT through ultrasonic method combined with shearing treatments, as described in previous literature [38–42]. 250 images of exfoliated MMT sheets were captured by atomic force microscope (AFM) so as to analysis the thickness distribution of 2D-MMT. Fig. 2a shows the thickness of original MMT was about 193.8 nm. Meanwhile, 2D-MMT of 1.44 nm in thickness was observed (Figs. 2c-2d), indicating the successful preparation of MMT nanosheets. As shown in Figs. 2e, 2D-MMT in thickness of 1–2 nm accounts for 56%, and 93.4% of the exfoliated MMT are less than 10 nm in thickness, demonstrating the well preparation of 2D-MMT nanosheets. A large reduction in thickness of MMT shell will be greatly beneficial to increase the content of PCM in composite.

Then, the 2D-MMT/SA composite with core-shell structure was produced through self-assembling the SA and 2D-MMT nanosheets. SA was added to SDS solution in which the ratio of SDS, SA and water is 1:15:100 by weight. This mixture solution was heated to 90 °C in order to melt SA, and then being stirred for 3 h. SA latex particles coated by SDS would be formed after the SA dispersion cooled down to room temperature. Next, the 2D-MMT layers mixed with CTAB were dispersed in water, and then this mixture with weight ratio of MMT: CTAB:

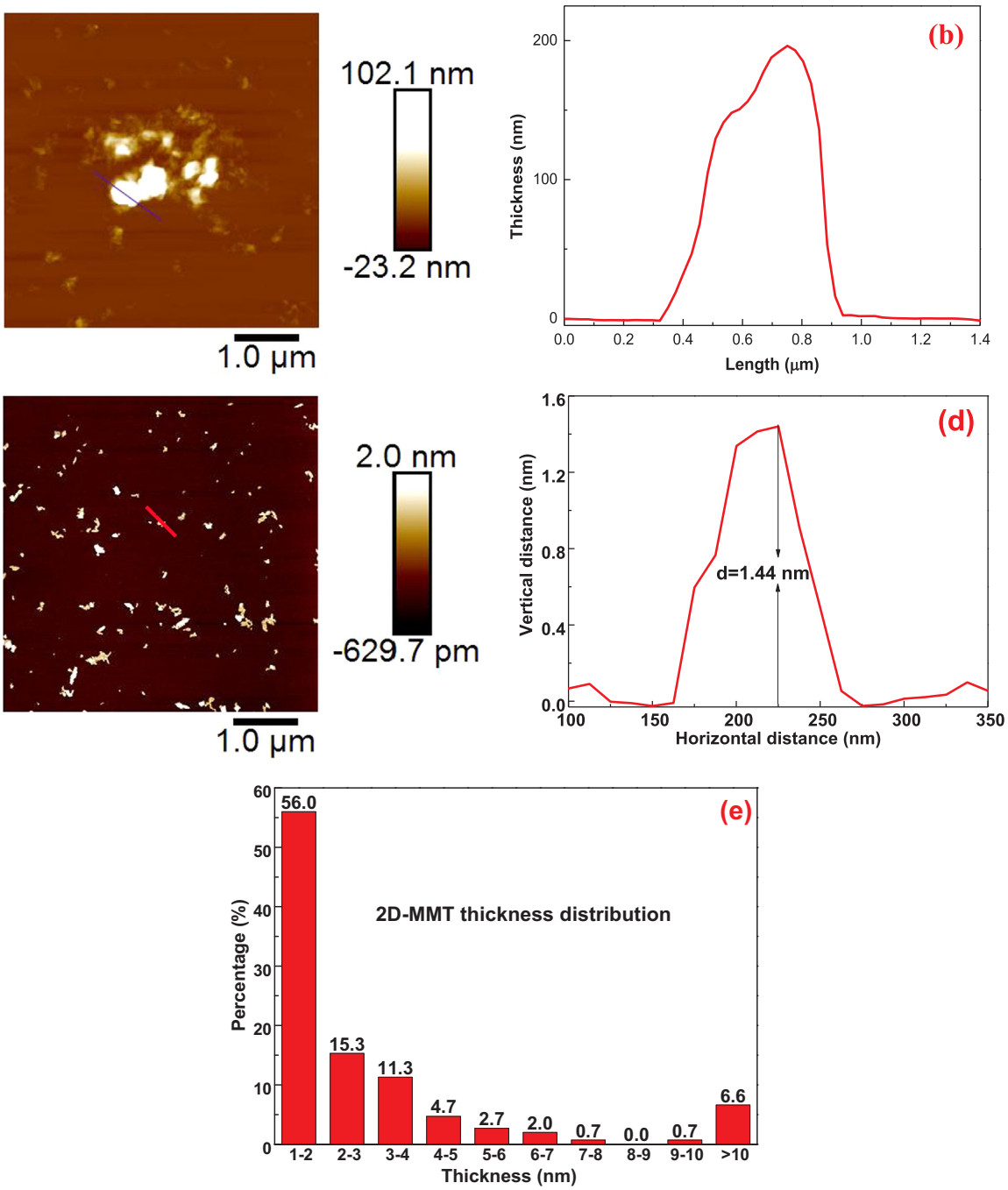

Fig. 2. Morphology and thickness of original MMT (a-b), morphology and thickness of 2D-MMT nanosheets (c-d), thickness distribution of 2D-MMT nanosheets (e).

water being 1:1:300 was stirred for about 2 h. Finally, SA latex particles solution was mixed with 2D-MMT dispersion modified by CTAB, followed by agitation for 1 h. After which the mixed solutions were filtrated, washed thoroughly and then dried at 50 °C in vacuum drying oven for 24 h to obtain 2D-MMT/SA composites. Three kinds of composites have been prepared in this work, the composite prepared by 1.5 g 2D-MMT and 15 g SA was called composite-1. Similarly, composites prepared by 2.1 g 2D-MMT + 15 g SA and 3.0 g 2D-MMT + 15 g SA were named composite-2 as well as composite-3 in turn.

Weight fraction of SA in 2D-MMT/SA composites in this work is calculated by Eq. (1):

$$\eta = \frac{\Delta H_{CPCM}}{\Delta H_{PCM}} \quad (1)$$

where ΔH_{CPCM} is the latent heat of the 2D-MMT/SA composite PCM, ΔH_{PCM} means the latent heat of pure SA PCM materials, while η represents the weight percentage of SA in 2D-MMT/SA composite.

2.3. Characterization

A D8 Advance X-ray diffractometer (Bruker, Germany) XRD pattern was used to measure the purity of MMT, 2θ ranged from 5° to 80° with a step scanning speed of $10^{\circ}min^{-1}$ were recorded in this work. Thickness of MMT nanosheets were determined through Multimode 8 at. force microscope (Bruker, Germany). The very diluted MMT nanosheets suspensions were instilled onto a newly cleaved mica surface so as to prepare the AFM measurement samples. And then AFM images of MMT nanosheets were captured with peak-force tapping mode. The thickness

of 250 exfoliated MMT nanosheets were obtained by Nanoscope Analysis software to analyze the thickness distribution.

Fourier transform infrared spectroscopy (FTIR) as well as zeta potential characterization analysis were performed to explore the self-assembly mechanism of 2D-MMT/SA composites. Infrared spectrum in the range of 4000–400 cm^{-1} was performed by using a Nexus FTIR spectrometer (Thermo Nicolet, US). Zeta potential measurements of the SA latex particles coated by SDS and the 2D-MMT modified by CTAB were measured by a Zetasizer Zeta-nano (Malven, UK) [43–45].

The microstructure and morphology of SA latex particles and 2D-MMT/SA composites were observed by Zeiss Uitra 55 Scanning electronic microscope (SEM) (Zeiss, Germany). Latent heat capacity of composite PCMs were measured by differential scanning calorimeter 8500 (DSC) (PE, US), while the thermal conductivity was measured by TPS2500S thermal constant analyzer (Hot Disk, Sweden). DSC measurements were performed at a heating rate of 1 ℃/min ranged from 30 to 85 ℃ in N_2 atmosphere.

Thermal cycling performances of the formed PCM composites were verified by heating/cooling cycling tests. Latent heats variations after dozens of thermal cycles were used to assess the thermal reliability of the composite PCM. The microstructure of composite PCM after heating/cooling cycling test was also observed through SEM measurements so as to evaluate the thermal and structural reliability.

3. Results and discussion

3.1. Structure characterization of 2D-MMT/SA

Fig. 3 displayed the FTIR spectrum of MMT, SA and 2D-MMT/SA composites. The FTIR of MMT are in accordance with many previous literatures, the 1641 cm^{-1} and 3624 cm^{-1} could be attributed to the vibration of –OH in MMT structure, while 464 cm^{-1} and 1032 cm^{-1} were ascribed to the Si-O bonds vibration [35]. Besides, the 3443 cm^{-1} were possibly assigned to the interlayer water of MMT. As for SA, the 719 cm^{-1} and 1472 cm^{-1} correspond to rocking vibration and deformation vibrations of -CH_2 and -CH_3. While 2849 cm^{-1} and 2917 cm^{-1} were due to the stretching vibrations of C-H [46]. Absorption band of 1704 cm^{-1} was on account of C=O vibrations [47].

In spectrum of 2D-MMT/SA composites, the bands at 463 and 1032 cm^{-1} correspond to MMT, while the bands appeared at 2955, 2917, 2849, 1704, 1471, 1298, 1103, 941, 719, 688 cm^{-1} were assigned to SA. The appearing of absorption band of MMT and SA at the same time proves that 2D-MMT and SA have been combined together successfully. On the other hand, no obvious new bands have been observed, demonstrating that MMT and SA in 2D-MMT/SA composites are just combined together through physical interactions.

To further illustrate detailed interaction mechanisms of the self-

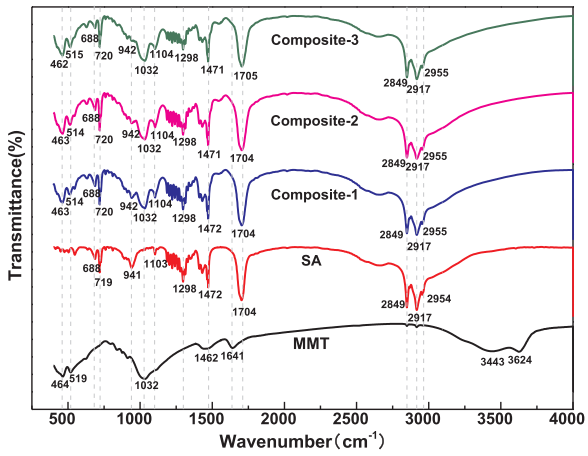

Fig. 3. FTIR spectra of SA, MMT and 2D-MMT/SA composites.

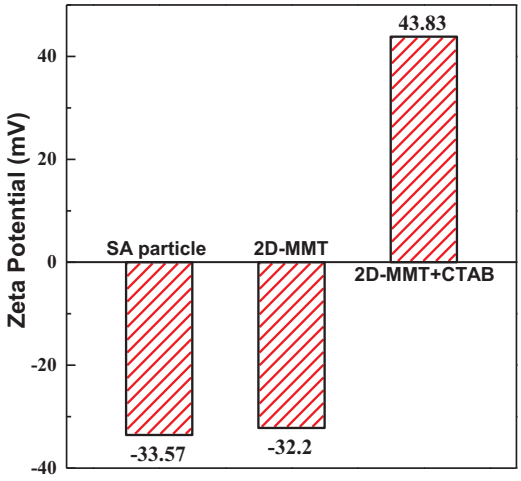

Fig. 4. Zeta potential of SA particles stabilized by SDS and 2D-MMT layers before and after adsorption of CTAB.

assembly of SA and 2D-MMT, the zeta potential has been measured. Fig. 4 illustrated the zeta potential of the SA latex particles and the 2D-MMT layers before and after adsorption of CTAB. SA latex particles were synthesized by adding SDS as a stabilizer, which allows the formation of the negative charged SA particles owing to the adsorption of SDS on the SA latex particle surface. Clearly, Fig. 4 shows a very negative zeta potential of the SA latex particles (− 33.57 mV). Meanwhile, the 2D-MMT layers renders the very positive surface charge (43.83 mV) after adsorption of CTAB. This observation demonstrates a strong electrostatic interaction between the SA latex particles and the modified 2D-MMT layers [44]. Combined with the FTIR results, we concluded that the SA particles and the 2D-MMT layers self-assemble to form a core-shell structural composite microcapsule PCM through strong electrostatic interaction.

Fig. 5a exhibits the SEM images of SA latex particles, which were applied as core materials. Figs. 5b-5d show the SEM of 2D-MMT/SA composites, which showed that the SA latex particles with smooth surfaces were tightly wrapped by the ultra-thin 2D-MMT nanosheets. The 2D-MMT nanosheets on the composites surface make a well-defined MMT nanosheets framework trapping SA inside. These SEM images of the composites demonstrated the successful preparation of composite PCM with core-shell structure. It was found that the core-shell structural 2D-MMT/SA composites maintains its shape even after filtering, washing and drying in the preparation process, which also demonstrated that the composite PCM self-assembled by 2D-MMT sheets on SA particles results in form-stable structure. Therefore, the composite PCM is structural stable and is reliable enough to hinder the leakage of PCM when melted.

Based on the results of FTIR, zeta potential and SEM, the synthetic process and the microstructure of 2D-MMT/SA composites were schematically illustrated. As shown in Fig. 6, the strong electrostatic forces between the MMT nanosheets and SA latex particles gives rise to the self-assembly of the core and shell materials, thus to form a microcapsules composites. This special structure of 2D-MMT/SA composite PCM provides stable 2D-MMT framework to prevent the leakage effectively. In addition, this composite has an ultra-high weight ratio of PCM core materials due to the very thin 2D-MMT shell materials, which show great promise in promoting the thermal energy storage capacity dramatically.

3.2. Thermal properties of 2D-MMT/SA

Thermal performances of composite PCM were measured through DSC and thermal constant analyzer. Fig. 7 displays the DSC curve of pure PCMs and 2D-MMT/SA composite PCMs. The endothermic peak of

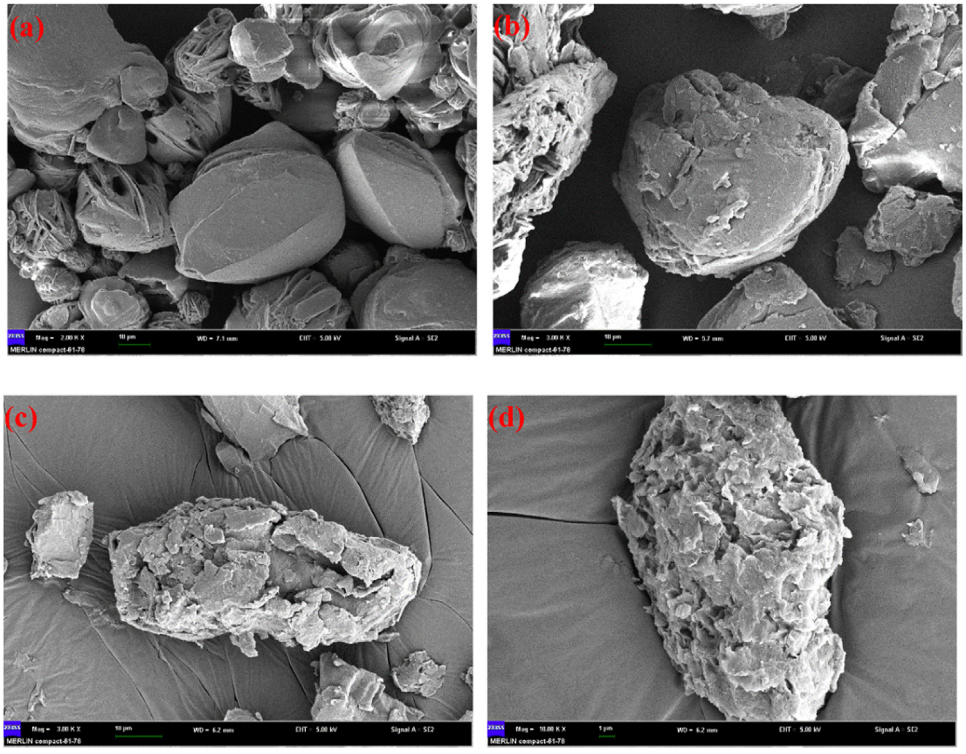

Fig. 5. SEM images of SA particles (a), composite-1 (b), composite-2 (c) and composite-3 (d).

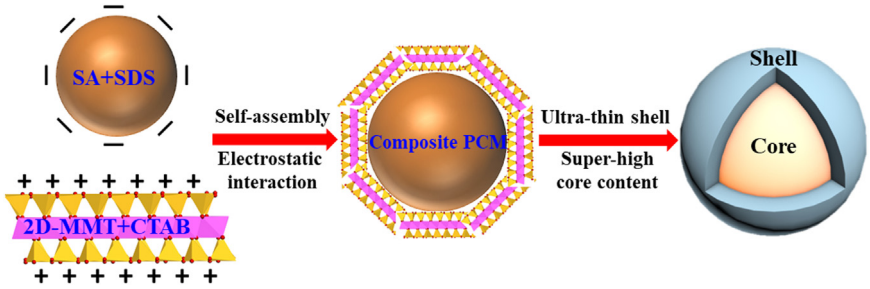

Fig. 6. Schematic illustration of the self-assembly of 2D-MMT layers and SA particles.

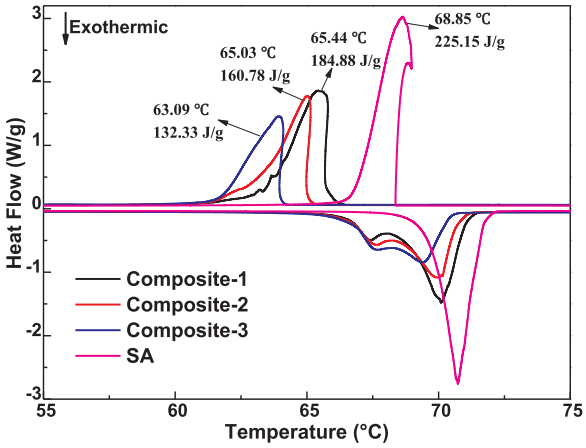

Fig. 7. DSC curve of SA and 2D-MMT/SA composites.

pure SA occurs at 68.85 °C, while the endothermic peak of composites occurs at 65.44 °C, 65.03 °C, and 63.09 °C, respectively. The slightly shift of phase change temperature may be due to the interactions between 2D-MMT and SA latex particles. These interactions may be the strong electrostatic interaction between SA and modified 2D-MMT, as demonstrated by our zeta potential measurement shown in Fig. 4. Besides, there may be some other interactions between SA core and 2D-MMT shell according to previous works, including hydrophobic attractions and H-bond interactions [27,35,48]. With respect to latent heat storage capacity, the latent heat of pure SA is 225.15 J/g, while the

Table 1
Comparison of latent heats of the 2D-MMT/SA composites with previous prepared MMT based composite PCMs.

Composite PCMs	Weight fraction of PCM (%)	Latent heat of melt (J/g)	Latent heat of freezing (J/g)	References
OMMT/paraffin	37.13	51.8	–	[49]
n-Octadecane/MMT/xGnp	31.82	80.16	78.78	[50]
OMMT/paraffin	29.4	37.78	–	[51]
RT20/MMT	39.97	53.6	–	[52]
SA/MMT	52.88	110	118	[35]
RT20/MMT	58	79.25	–	[53]
Paraffin/HDPE/OMMT	59.74	99.78	–	[54]
n-hexadecane/MMT	60	126	125	[27]
2D-MMT/SA	**82.11**	**184.88**	**181.04**	This work

Table 2
Comparison of latent heats of the 2D-MMT/SA composites with previous prepared composite PCMs using SA.

Composite PCMs	Weight fraction of PCM (%)	Latent heat of melt (J/g)	Latent heat of freezing (J/g)	References
SA@MWCNT	46.74	91.94	92.55	[55]
SA/Co_3O_4	81.82	183.81	189.81	[56]
SA/rGO/MOF	72.62	142.4	138.1	[57]
SA/EG	–	148.14	152.10	[58]
SA/SiO_2	70	135.3	133.5	[59]
2D-MMT/SA	**82.11**	**184.88**	**181.04**	This work

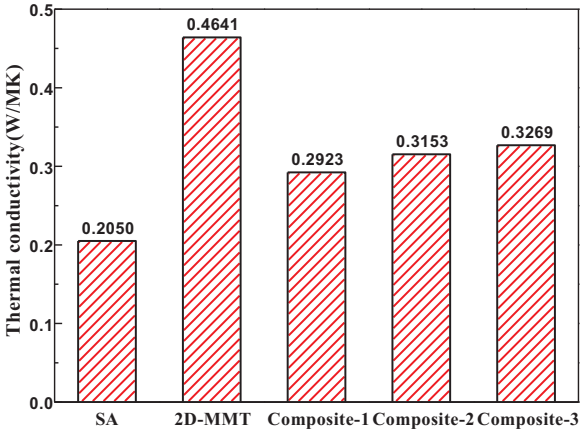

Fig. 8. Thermal conductivity of MMT, SA and their composites.

thermal energy storage of composite-1 to composite-3 are 184.88 J/g, 160.78 J/g and 132.33 J/g, respectively. For the composite-1 which was prepared by 1.5 g 2D-MMT and 15 g SA, the mass fraction η of SA in the 2D-MMT/SA composite is 82.11% calculated according to Eq. (1). Compared with PCM composites prepared by MMT in previous literatures, the latent heat of 2D-MMT/SA composites in this work shows obvious advantages over the reported paper. As shown in Table 1, the highest weight fraction of PCM was 82.11% and latent heat of PCM composite was 184.88 J/g in this work. The 2D-MMT/SA composite PCM prepared in this work shows very large latent heat capacity, far higher than that MMT based composite PCM in previous literature. Compared with other shape-stabilized PCMs using SA, 2D-MMT/SA prepared in this work still shows superior performance in latent heat capacity, as displayed in Table 2. Therefore, this 2D-MMT/SA composite PCMs are believed to be potential for thermal energy storage in sustainable energy field, such as utilizing of solar energy and recovering industrial waste heat.

Fig. 8 displays the thermal conductivity of SA, 2D-MMT layers and their composites. Thermal conductivity of composite PCM prepared using 1.5 g 2D-MMT increases to 142.59% of SA. Besides, the composite

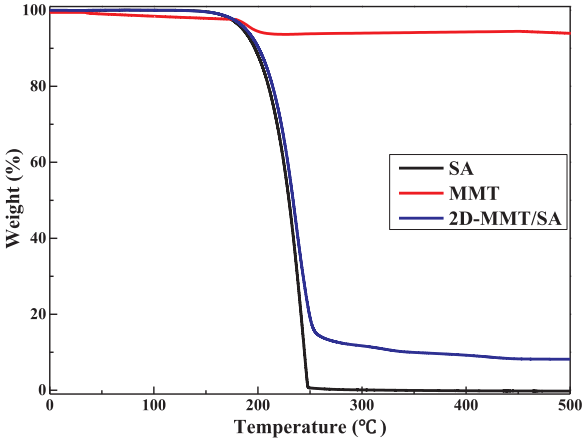

Fig. 10. TGA curves of 2D-MMT, SA and 2D-MMT/SA composite-1.

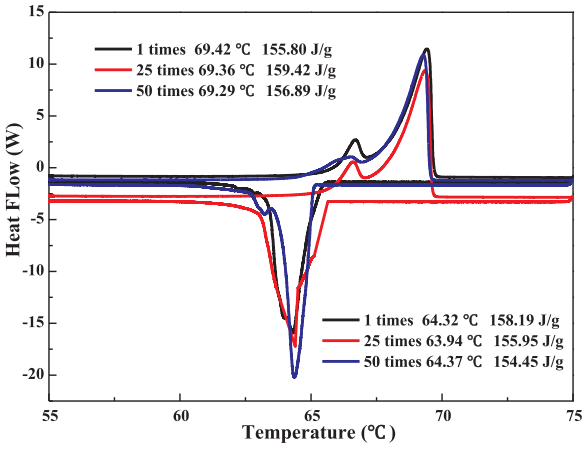

Fig. 11. DSC curve of 2D-MMT/SA composite-2 over 25 and 50 heating/cooling cycles.

prepared with 2.1 g 2D-MMT layers increases the thermal conductivity to 153.80% of SA. Meanwhile, the composite PCM prepared with 3 g 2D-MMT showed a promotion of 159.46% of SA in thermal conductivity. On one hand, the relatively large improvement of the thermal conductivity can be explained by relative high heat-conducting property of 2D-MMT layers. On the other hand, the 2D-MMT framework and the micron size of PCM composites results to very large heat transfer area, which may also contribute to the promotion of the thermal conductivity.

3.3. Thermal and structure stability of 2D-MMT/SA

The morphologies of pure SA and the 2D-MMT/SA composite PCM heated at 80 °C (higher than the melting point of SA (~70 °C)) were

Fig. 9. Thermal stability measurements.

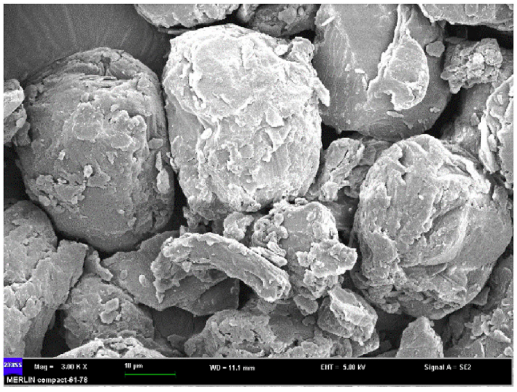

Fig. 12. SEM images of 2D-MMT/SA composites after 40 heating/cooling cycles.

showed in Fig. 9. It is clearly to observe that the SA particles melt to liquid quickly, while no leakage was found on the 2D-MMT/SA composites, even only 1.5 g 2D-MMT was used to encapsulate the SA particles. Thus, a very low dosage of MMT is enough to prevent leakage when SA change phase to liquid. In addition, the composites keep their shape stable even at high temperature, which indicates that the simple self-assembly of SA latex particles and modified MMT layers is a simple and convenient method to synthesize form-stable composites with microcapsule structure. This core-shell structural 2D-MMT/SA composite PCMs provide a strong shell frame to trap core SA inside, which is beneficial to the restriction of leakage.

Thermal stability has also been examined by TGA measurements. As shown in Fig. 10, SA began to decompose at around 180 ℃, and almost all the SA were decomposed at around 250 ˚C. As for the 2D-MMT, only the removal of adsorption water in MMT structure occurred at around 100–200 ˚C. Besides, the 2D-MMT/SA composites prepared in this work showed a good thermal stability because no decomposition was found below 180 ˚C, suggesting that the 2D-MMT materials are suitable for preparing PCMs composites. On the other hand, the 2D-MMT shows a weight loss due to the dehydration process, the weight loss of 2D-MMT occupies approximately 9%. From the TGA curve of 2D-MMT/SA, the weight loss accounts for about 93% including the dehydration of MMT and the decomposition of SA. This mass ratio of PCM in composite PCMs measured by TGA is only slightly higher than that value measured from DSC. But it can still be concluded that the mass fraction of SA in the composites agrees well with the results calculated from DSC.

3.4. Cycling performance of 2D-MMT/SA

Fig. 11 shows the DSC curve of 2D-MMT/SA composites over 25 and 50 heating/cooling cycles. It is obvious that this 2D-MMT/SA composite PCM exhibits a stable cycling behaviors, which indicates that no chemical degradation or segregation of SA and 2D-MMT took place during heating/cooling tests. Only very slight changes of latent heats (± 4 J/g) and phase change temperature (± 0.5 ˚C) of 2D-MMT/SA have been observed, which are in the normal range of DSC measurement errors (± 0.3%). Besides, this very little change of phase change properties that can be ignored also demonstrates a high structural and thermal stability of this composite PCMs. In addition, these negligible phase change temperature and latent heat does not affect the practical applications of this composite PCMs at all. Therefore, the 2D-MMT/SA composite PCM with good thermal durability and excellent cycling performance turns out to be applicable for solar thermal storage field.

Fig. 12. Shows the SEM images of 2D-MMT/SA composites after 40 heating/cooling cycles. It is clearly observed that, even after 50 times thermal cycling, the PCM microcapsules still keep good shape, no destruction or no separation between the SA and 2D-MMT layers has taken place. Thus, the synthetic 2D-MMT/SA has very good structure stability as well as excellent thermal cycling performance. In consequence, it is demonstrated that the 2D-MMT/SA composites prepared in this work shows ultra-high thermal energy storage capacity, promoted thermal conductivity, excellent structure stability and outstanding cycling performance, which are of tremendous potential for solar thermal energy storage in sustainable energy field.

4. Conclusions

(1) The 2D-MMT/SA composites with a core-shell structure are self-assembled through strong electrostatic interaction.
(2) The 2D-MMT/SA composites have an ultra-high weight fraction (> 80%) of SA due to the very thin MMT nanosheets shell, thus to provide tremendous latent heat storage capacity (184.88 J/g).
(3) The protective 2D-MMT shell gives an excellent structure stability to the composite and is effective to restrict leakage of PCM during phase transition process.
(4) The relatively high thermal conductivity of MMT nanosheets results in an improved thermal conductivity of the 2D-MMT/SA composite PCM.
(5) The 2D-MMT/SA composite exhibits a stable cycling performance in the heating/cooling test and shows great promise for sustainable energy applications.

Acknowledgements

The financial supports to this work from the National Natural Science Foundation of China under the projects Nos. 51674183 and 51874220 are gratefully acknowledged. This research is also supported by the Natural Science Foundation of Hubei Province of China (2018CFB468).

References

[1] W. Peng, H. Li, S. Song, Synthesis of fluorinated graphene/coal-layered double hydroxide composites as electrode materials for supercapacitors, ACS Appl. Mater. Interfaces 9 (2017) 5204–5212, https://doi.org/10.1021/acsami.6b11316.
[2] X. Huang, X. Chen, A. Li, D. Atinafu, H. Gao, W. Dong, G. Wang, Shape-stabilized phase change materials based on porous supports for thermal energy storage applications, Chem. Eng. J. 356 (2019) 641–661, https://doi.org/10.1016/j.cej.2018.09.013.
[3] N. Putra, M. Amin, E.A. Kosasih, R.A. Luanto, N.A. Abdullah, Characterization of the thermal stability of RT 22 HC/graphene using a thermal cycle method based on thermoelectric methods, Appl. Therm. Eng. 124 (2017) 62–70, https://doi.org/10.1016/j.applthermaleng.2017.06.009.
[4] R.J. Warzoha, A.S. Fleischer, Effect of carbon nanotube interfacial geometry on thermal transport in solid-liquid phase change materials, Appl. Energy 154 (2015) 271–276, https://doi.org/10.1016/j.apenergy.2015.04.121.
[5] Y. Li, S. Yu, P. Chen, R. Rojas, A. Hajian, L. Berglund, Cellulose nanofibers enable paraffin encapsulation and the formation of stable thermal regulation nanocomposites, Nano Energy 34 (2017) 541–548, https://doi.org/10.1016/j.nanoen.2017.03.010.
[6] C. Chen, H. Ling, Z. (John) Zhai, Y. Li, F. Yang, F. Han, S. Wei, Thermal performance of an active-passive ventilation wall with phase change material in solar greenhouses, Appl. Energy 216 (2018) 602–612, https://doi.org/10.1016/j.apenergy.2018.02.130.
[7] C. Finck, R. Li, R. Kramer, W. Zeiler, Quantifying demand flexibility of power-to-heat and thermal energy storage in the control of building heating systems, Appl. Energy 209 (2018) 409–425, https://doi.org/10.1016/j.apenergy.2017.11.036.
[8] M. Amin, N. Putra, E.A. Kosasih, E. Prawiro, R.A. Luanto, T.M.I. Mahlia, Thermal properties of beeswax/graphene phase change material as energy storage for building applications, Appl. Therm. Eng. 112 (2017) 273–280, https://doi.org/10.1016/j.applthermaleng.2016.10.085.
[9] G. Jiang, J. Huang, Y. Fu, M. Cao, M. Liu, Thermal optimization of composite phase change material/expanded graphite for Li-ion battery thermal management, Appl. Therm. Eng. 108 (2016) 1119–1125, https://doi.org/10.1016/j.applthermaleng.2016.07.197.
[10] A. Karaipekli, A. Biçer, A. Sarı, V.V. Tyagi, Thermal characteristics of expanded perlite/paraffin composite phase change material with enhanced thermal conductivity using carbon nanotubes, Energy Convers. Manag. 134 (2017) 373–381, https://doi.org/10.1016/j.enconman.2016.12.053.
[11] L. Zhang, R. Li, B. Tang, P. Wang, Solar-thermal conversion and thermal energy storage of graphene foam-based composites, Nanoscale 8 (2016) 14600–14607, https://doi.org/10.1039/C6NR03921A.
[12] S.G. Sarwat, P. Gehring, G. Rodriguez Hernandez, J.H. Warner, G.A.D. Briggs,

J.A. Mol, H. Bhaskaran, Scaling limits of graphene nanoelectrodes, Nano Lett. 17 (2017) 3688–3693, https://doi.org/10.1021/acs.nanolett.7b00909.
[13] Y. Yuan, N. Zhang, T. Li, X. Cao, W. Long, Thermal performance enhancement of palmitic-stearic acid by adding graphene nanoplatelets and expanded graphite for thermal energy storage: a comparative study, Energy 97 (2016) 488–497, https://doi.org/10.1016/j.energy.2015.12.115.
[14] S. Harish, D. Orejon, Y. Takata, M. Kohno, Thermal conductivity enhancement of lauric acid phase change nanocomposite with graphene nanoplatelets, Appl. Therm. Eng. 80 (2015) 205–211, https://doi.org/10.1016/j.applthermaleng.2015.01.056.
[15] R. Chen, Y. Cui, H. Tian, R. Yao, Z. Liu, Y. Shu, C. Li, Y. Yang, T. Ren, G. Zhang, R. Zou, Controllable thermal rectification realized in binary phase change composites, Sci. Rep. 5 (2015) 1–8, https://doi.org/10.1038/srep08884.
[16] Y. Xu, A.S. Fleischer, G. Feng, Reinforcement and shape stabilization of phase-change material via graphene oxide aerogel, Carbon N. Y. 114 (2017) 334–346, https://doi.org/10.1016/j.carbon.2016.11.069.
[17] M. Mehrali, S. Tahan Latibari, M. Mehrali, T.M.I. Mahlia, E. Sadeghinezhad, H.S.C. Metselaar, Preparation of nitrogen-doped graphene/palmitic acid shape stabilized composite phase change material with remarkable thermal properties for thermal energy storage, Appl. Energy 135 (2014) 339–349, https://doi.org/10.1016/j.apenergy.2014.08.100.
[18] W.S. Kang, K.Y. Rhee, S.J. Park, Thermal, impact and toughness behaviors of expanded graphite/graphite oxide-filled epoxy composites, Compos. Part B Eng. 94 (2016) 238–244, https://doi.org/10.1016/j.compositesb.2016.03.052.
[19] Q. Lian, K. Li, A.A.S. Sayyed, J. Cheng, J. Zhang, Study on a reliable epoxy-based phase change material: facile preparation, tunable properties, and phase/microphase separation behavior, J. Mater. Chem. A 5 (2017) 14562–14574, https://doi.org/10.1039/C7TA02816D.
[20] M. Mehrali, S.T. Latibari, M. Mehrali, T.M. Indra Mahlia, H.S. Cornelis Metselaar, Preparation and properties of highly conductive palmitic acid/graphene oxide composites as thermal energy storage materials, Energy 58 (2013) 628–634, https://doi.org/10.1016/j.energy.2013.05.050.
[21] Z. Chen, J. Wang, F. Yu, Z. Zhang, X. Gao, Preparation and properties of graphene oxide-modified poly(melamine-formaldehyde) microcapsules containing phase change material n-dodecanol for thermal energy storage, J. Mater. Chem. A 3 (2015) 11624–11630, https://doi.org/10.1039/C5TA01852H.
[22] A.R. Akhiani, M. Mehrali, S. Tahan Latibari, M. Mehrali, T.M.I. Mahlia, E. Sadeghinezhad, H.S.C. Metselaar, One-step preparation of form-stable phase change material through self-assembly of fatty acid and graphene, J. Phys. Chem. C 119 (2015) 22787–22796, https://doi.org/10.1021/acs.jpcc.5b06089.
[23] J. Wang, X. Huang, H. Gao, A. Li, C. Wang, Construction of CNT@Cr-MIL-101-NH2hybrid composite for shape-stabilized phase change materials with enhanced thermal conductivity, Chem. Eng. J. 350 (2018) 164–172, https://doi.org/10.1016/j.cej.2018.05.190.
[24] Y. Hu, S. Song, A. Lopez-Valdivieso, Effects of oxidation on the defect of reduced graphene oxides in graphene preparation, J. Colloid Interface Sci. 450 (2015) 68–73, https://doi.org/10.1016/j.jcis.2015.02.059.
[25] H. Yi, X. Zhang, Y. Zhao, Y. Liu, S. Song, A novel method for the quantitative determination of defects on graphene surfaces, J. Colloid Interface Sci. 499 (2017) 62–66, https://doi.org/10.1016/j.jcis.2017.03.094.
[26] A. Li, J. Wang, C. Dong, W. Dong, D.G. Atinafu, X. Chen, H. Gao, G. Wang, Core-sheath structural carbon materials for integrated enhancement of thermal conductivity and capacity, Appl. Energy 217 (2018) 369–376, https://doi.org/10.1016/j.apenergy.2017.12.106.
[27] N. Sarier, E. Onder, S. Ozay, Y. Ozkilic, Preparation of phase change material-montmorillonite composites suitable for thermal energy storage, Thermochim. Acta 524 (2011) 39–46, https://doi.org/10.1016/j.tca.2011.06.009.
[28] W. Wang, Y. Zhao, H. Bai, T. Zhang, V. Ibarra-Galvan, S. Song, Methylene blue removal from water using the hydrogel beads of poly(vinyl alcohol)-sodium alginate-chitosan-montmorillonite, Carbohydr. Polym. 198 (2018) 518–528, https://doi.org/10.1016/j.carbpol.2018.06.124.
[29] X. Zhang, H. Yi, Y. Zhao, F. Min, S. Song, Study on the differences of Na- and Ca-montmorillonites in crystalline swelling regime through molecular dynamics simulation, Adv. Powder Technol. 27 (2016) 779–785, https://doi.org/10.1016/j.apt.2016.03.005.
[30] H. Yi, X. Zhang, Y. Zhao, L. Liu, S. Song, Molecular dynamics simulations of hydration shell on montmorillonite (001) in water, Surf. Interface Anal. 48 (2016) 976–980, https://doi.org/10.1002/sia.6000.
[31] H. Li, S. Song, X. Dong, F. Min, Y. Zhao, C. Peng, Y. Nahmad, Molecular dynamics study of crystalline swelling of montmorillonite as affected by interlayer cation hydration, JOM 70 (2017) 479–484, https://doi.org/10.1007/s11837-017-2666-2.
[32] S. Kang, Y. Zhao, W. Wang, T. Zhang, T. Chen, H. Yi, F. Rao, S. Song, Removal of methylene blue from water with montmorillonite nanosheets/chitosan hydrogels as adsorbent, Appl. Surf. Sci. 448 (2018) 203–211, https://doi.org/10.1016/J.APSUSC.2018.04.037.
[33] H. Yi, F. Jia, Y. Zhao, W. Wang, S. Song, H. Li, C. Liu, Surface wettability of montmorillonite (0 0 1) surface as affected by surface charge and exchangeable cations: a molecular dynamic study, Appl. Surf. Sci. 459 (2018) 148–154, https://doi.org/10.1016/j.apsusc.2018.07.216.
[34] C. Liu, Z. Rao, J. Zhao, Y. Huo, Y. Li, Review on nanoencapsulated phase change materials: preparation, characterization and heat transfer enhancement, Nano Energy 13 (2015) 814–826, https://doi.org/10.1016/j.nanoen.2015.02.016.
[35] K. Peng, L. Fu, X. Li, J. Ouyang, H. Yang, Stearic acid modified montmorillonite as emerging microcapsules for thermal energy storage, Appl. Clay Sci. 138 (2017) 100–106, https://doi.org/10.1016/j.clay.2017.01.003.
[36] P. Sittisart, M.M. Farid, Fire retardants for phase change materials, Appl. Energy 88 (2011) 3140–3145, https://doi.org/10.1016/j.apenergy.2011.02.005.
[37] Y. Cai, Y. Hu, L. Song, Q. Kong, R. Yang, Y. Zhang, Z. Chen, W. Fan, Preparation and flammability of high density polyethylene/paraffin/organophilic montmorillonite hybrids as a form stable phase change material, Energy Convers. Manag. 48 (2007) 462–469, https://doi.org/10.1016/j.enconman.2006.06.021.
[38] T. Chen, Y. Zhao, S. Song, Correlation of electrophoretic mobility with exfoliation of montmorillonite platelets in aqueous solutions, Colloids Surf. A Physicochem. Eng. Asp. 525 (2017) 1–6, https://doi.org/10.1016/j.colsurfa.2017.04.057.
[39] X. Zhang, H. Yi, H. Bai, Y. Zhao, F. Min, S. Song, Correlation of montmorillonite exfoliation with interlayer cations in the preparation of two-dimensional nanosheets, RSC Adv. 7 (2017) 41471–41478, https://doi.org/10.1039/C7RA07816A.
[40] Y. Zhao, H. Yi, F. Jia, H. Li, C. Peng, S. Song, A novel method for determining the thickness of hydration shells on nanosheets: a case of montmorillonite in water, Powder Technol. 306 (2017) 74–79, https://doi.org/10.1016/j.powtec.2016.10.045.
[41] W. Wang, Y. Zhao, H. Yi, T. Chen, S. Kang, H. Li, S. Song, Preparation and characterization of self-assembly hydrogels with exfoliated montmorillonite nanosheets and chitosan, Nanotechnology 29 (2018), https://doi.org/10.1088/1361-6528/aa9ba4.
[42] T. Chen, Y. Yuan, Y. Zhao, F. Rao, S. Song, Effect of layer charges on exfoliation of montmorillonite in aqueous solutions, Colloids Surf. A Physicochem. Eng. Asp. 548 (2018) 92–97, https://doi.org/10.1016/j.colsurfa.2018.03.066.
[43] C. Liu, W. Zhang, S. Song, H. Li, A novel method to improve carboxymethyl cellulose performance in the flotation of talc, Miner. Eng. 131 (2019) 23–27, https://doi.org/10.1016/j.mineng.2018.11.003.
[44] T. Chen, Y. Zhao, S. Song, Electrophoretic mobility study for heterocoagulation of montmorillonite with fluorite in aqueous solutions, Powder Technol. 309 (2017) 61–67, https://doi.org/10.1016/j.powtec.2016.12.086.
[45] C. Liu, G. Ai, S. Song, The effect of amino trimethylene phosphonic acid on the flotation separation of pentlandite from lizardite, Powder Technol. 336 (2018) 527–532, https://doi.org/10.1016/j.powtec.2018.06.030.
[46] T.D. Dao, H.M. Jeong, Novel stearic acid/graphene core-shell composite microcapsule as a phase change material exhibiting high shape stability and performance, Sol. Energy Mater. Sol. Cells 137 (2015) 227–234, https://doi.org/10.1016/j.solmat.2015.02.009.
[47] S. Liu, H. Yang, Stearic acid hybridizing coal-series kaolin composite phase change material for thermal energy storage, Appl. Clay Sci. 101 (2014) 277–281, https://doi.org/10.1016/j.clay.2014.09.002.
[48] P. Lv, C. Liu, Z. Rao, Review on clay mineral-based form-stable phase change materials: preparation, characterization and applications, Renew. Sustain. Energy Rev. 68 (2017) 707–726, https://doi.org/10.1016/j.rser.2016.10.014.
[49] M. Li, Q. Guo, S. Nutt, Carbon nanotube/paraffin/montmorillonite composite phase change material for thermal energy storage, Sol. Energy 146 (2017) 1–7, https://doi.org/10.1016/j.solener.2017.02.003.
[50] S.-G. Jeong, S. Jin Chang, S. We, S. Kim, Energy efficient thermal storage montmorillonite with phase change material containing exfoliated graphite nanoplatelets, Sol. Energy Mater. Sol. Cells 139 (2015) 65–70, https://doi.org/10.1016/j.solmat.2015.03.010.
[51] H. Kao, M. Li, X. Lv, J. Tan, Preparation and thermal properties of expanded graphite/paraffin/organic montmorillonite composite phase change material, J. Therm. Anal. Calorim. 107 (2012) 299–303, https://doi.org/10.1007/s10973-011-1520-y.
[52] X. Fang, Z. Zhang, Z. Chen, Study on preparation of montmorillonite-based composite phase change materials and their applications in thermal storage building materials, Energy Convers. Manag. 49 (2008) 718–723, https://doi.org/10.1016/j.enconman.2007.07.031.
[53] X. Fang, Z. Zhang, A novel montmorillonite-based composite phase change material and its applications in thermal storage building materials, Energy Build. 38 (2006) 377–380, https://doi.org/10.1016/j.enbuild.2005.07.005.
[54] Y. Cai, L. Song, Q. He, D. Yang, Y. Hu, Preparation, thermal and flammability properties of a novel form-stable phase change materials based on high density polyethylene/poly(ethylene-co-vinyl acetate)/organophilic montmorillonite nanocomposites/paraffin compounds, Energy Convers. Manag. 49 (2008) 2055–2062, https://doi.org/10.1016/j.enconman.2008.02.013.
[55] Y. Chen, Q. Zhang, X. Wen, H. Yin, J. Liu, A novel CNT encapsulated phase change material with enhanced thermal conductivity and photo-thermal conversion performance, Sol. Energy Mater. Sol. Cells 184 (2018) 82–90, https://doi.org/10.1016/j.solmat.2018.04.034.
[56] D. Li, X. Cheng, Y. Li, H. Zou, G. Yu, G. Li, Y. Huang, Effect of MOF derived hierarchical Co_3O_4/expanded graphite on thermal performance of stearic acid phase change material, Sol. Energy 171 (2018) 142–149, https://doi.org/10.1016/j.solener.2018.06.062.
[57] A. Li, C. Dong, W. Dong, D.G. Atinafu, H. Gao, X. Chen, G. Wang, Hierarchical 3D reduced graphene porous-carbon-based PCMs for superior thermal energy storage performance, ACS Appl. Mater. Interfaces 10 (2018) 32093–32101, https://doi.org/10.1021/acsami.8b09541.
[58] J.L. Zhang, N. Wu, X.W. Wu, Y. Chen, Y. Zhao, J.F. Liang, X.B. Bai, High latent heat stearic acid impregnated in expanded graphite, Thermochim. Acta 663 (2018) 118–124, https://doi.org/10.1016/j.tca.2018.03.018.
[59] S. Fan, H. Gao, W. Dong, J. Tang, J. Wang, M. Yang, G. Wang, Shape-stabilized phase change materials based on stearic acid and mesoporous hollow SiO_2 microspheres (SA/SiO2) for thermal energy storage, Eur. J. Inorg. Chem. 2017 (2017) 2138–2143, https://doi.org/10.1002/ejic.201601380.